INSTITUTE OF PHYSICS PUBLISHING PLASMA PHYSICS AND CONTROLLED FUSION

Plasma Phys. Control. Fusion **48** (2006) B359–B369 doi:10.1088/0741-3335/48/12B/S33

The effect of ECRH on the electron velocity distribution function

S Coda, I Klimanov, S Alberti, G Arnoux[1], P Blanchard, A Fasoli and the TCV team[2]

Ecole Polytechnique Fédérale de Lausanne (EPFL), Centre de Recherches en Physique des Plasmas, Association Euratom–Confédération Suisse, EPFL SB CRPP, Station 13, CH–1015 Lausanne, Switzerland

E-mail: stefano.coda@epfl.ch

Received 23 June 2006
Published 14 November 2006
Online at stacks.iop.org/PPCF/48/B359

Abstract

Electron cyclotron resonance heating (ECRH) is a mature technology that has progressed constantly over a period of forty years, particularly as a tool in magnetic confinement fusion. As with other heating methods, this technique has seen a steady increase in the sophistication of its applications, from bulk heating through profile tailoring and finally to distribution function engineering. By comparison with other techniques, ECRH presents the significant advantages of good coupling, localized power deposition, easy launching and precise directionality. This paper reviews some recent applications related to third harmonic ECRH and highlights the role of the relaxation dynamics of suprathermal electrons, both in real space and in velocity space, in regulating the overall effect of ECRH on fusion plasmas. A technique for direct visualization of these relaxation phenomena, using modulated ECRH, is described and demonstrated.

(Some figures in this article are in colour only in the electronic version)

1. Introduction

As magnetic confinement fusion sets its sights on the goal of partial or total reaction self-sustainment—a key step towards concrete energy generation—the function of external power sources shifts from bulk plasma heating to the sustainment of optimized plasma distribution functions. In particular, to the 'tailoring' of spatial profiles (of temperature, current, density,

[1] Current address: Département de Recherches sur la Fusion Contrôlée, Association EURATOM–CEA, CEA/Cadarache, 13108 Saint Paul-lez-Durance Cédex, France

[2] See author list in Goodman T P *et al* 2005 *Plasma Phys. Control. Fusion* **47** B107.

etc) for the purpose of improving confinement or stability, the task of momentum space 'engineering' is gradually being added. Indeed, in any driven system, breaking the tight bonds of thermodynamic equilibrium opens the possibility of population inversion—a stable non-equilibrium state with optimal properties for a specific goal: in this case, efficient fusion reactivity or plasma current generation. Electromagnetic waves are an especially effective tool to this end, as lower hybrid current drive experiments proved well over twenty years ago [1].

More recently, progress in high power millimetre wave generation [2, 3] has brought the technique of electron cyclotron resonance heating (ECRH) to the fore [4, 5], its short wavelength and unique localization and directionality properties affording an unprecedented degree of phase space manipulation. The control of MHD stability by localized deposition on or near resonant surfaces [6] has become one of the main new application avenues for ECRH and ECCD (electron cyclotron current drive) in the past ten to fifteen years. In particular, control of the sawtooth instability in tokamaks is achieved either by global control of the current profile [7] or by accurate deposition in the vicinity of the q=1 surface, resulting in large controllable variations in the sawtooth period [8, 9], which in turn have secondary effects on the excitation of other MHD modes such as neoclassical tearing modes (NTMs) through mode coupling. Direct control of NTMs has also been demonstrated through targeting of the associated magnetic island [10, 11]. A more global form of profile control is applied to the sustainment of fully non-inductive discharges, in which the entire current profile is determined by the ECCD distribution [12].

The resonance condition for electron cyclotron waves involves both spatial and momentum coordinates. That is, the resonant electrons at a given spatial location are confined to a specific region in velocity space. This engenders the possibility of momentum space tailoring. The sustainment of fully non-inductive electron internal transport barriers [8, 13, 14] is an emblematic example of the new approach to full distribution function manipulation, combining velocity space control (by Fisch–Boozer current drive [15]) with real space control (by safety factor profile inversion) to sustain a hollow current density profile and enhance the fusion performance through the associated reduction of transport. A positive synergy between ECRH and lower hybrid current drive has also been observed owing to a favourable interplay of the resonant locations in velocity space [16]. Even more advanced applications are appearing on the horizon, such as the possibility of using the Ohkawa current drive mechanism [17] (a reversal of the Fisch–Boozer effect caused by the rapid redistribution of momentum by electrons trapped in a magnetic well) for efficient current generation at far off-axis locations in tokamaks [18].

The effect of ECRH on the electron distribution function (e.d.f.) is studied through experimental measurements and modelling codes. A few diagnostic techniques are especially suited for identifying the departure of the e.d.f. from the equilibrium Maxwellian shape. Measurements of hard x-ray emission at energies well above the thermal energy have been extensively used to detect the presence of suprathermal electrons [19–21] also specifically as a result of applying ECRH or ECCD [22–24]. Localization can be achieved, especially in tomographic arrangements [21], but a unique reconstruction of the electron energy distribution is not possible without strong *a priori* assumptions. Photon statistics also tend to limit the temporal resolution and generally preclude perturbative low power studies [25]. Electron cyclotron emission (ECE) can be a very sensitive detector of suprathermal populations in geometries that place resonant suprathermal electrons closer to the receiving antenna than the thermal population. Such geometries include high field side [26, 27], vertical [28, 29] and toroidally oblique detection [30]. More recently, the perturbation by suprathermal electrons of the bulk temperature measurement performed by Thomson scattering [31] has been proposed as a diagnostic of near-Maxwellian e.d.f. deformations in conjunction with

ECE measurements [32]. Finally, Langmuir probes [33] and spectroscopic techniques [34] have also yielded information on the e.d.f. in the low temperature plasma edge.

On the numerical code front, the premier tool for following the e.d.f. evolution has been the quasilinear Fokker–Planck model, which has been implemented in numerous variants around the world [35–37]. Recent efforts in the direction of fully nonlinear modelling have employed a Monte Carlo technique [38].

This paper will discuss the effect of ECRH on the e.d.f. in the TCV device [39], whose very high power density has enabled particularly stringent tests of the potential of ECRH as a phase space control tool. In particular, third harmonic EC absorption, and its interplay with the existence of a non-Maxwellian e.d.f., will be discussed in section 2. Section 3 will review our current understanding of the relaxation dynamics of the suprathermal population, which act to regulate the overall effect of ECRH on the e.d.f.. Conclusions will be offered at the end of the paper.

2. Absorption of third harmonic ECRH

The remainder of this paper will focus on experimental results obtained on the tokamak TCV [39] (major radius $R = 0.88$ cm, minor radius $a = 0.25$ cm, plasma current $I_p \leqslant 1$ MA, toroidal magnetic field $B_\phi \leqslant 1.54$ T), which is equipped with a second harmonic (X2, 82.7 GHz) ECRH/ECCD system composed of six 0.5 MW beams launched by independently steerable lateral launchers, and a third harmonic (X3, 118 GHz) system with three 0.5 MW beams launched vertically by a single launcher from the top of the vessel [40].

The purpose of the X3 apparatus is to heat plasmas of higher density (up to 1.15×10^{20} m^{-3}) than is accessible by X2 [41]; the vertical launching geometry aims at maximizing first pass absorption, which is a decreasing function of the harmonic number, by maximizing the length of the interaction region. The launching mirror can be moved in the radial direction and rotated in the poloidal plane. The $1/\gamma$ dependence of the cyclotron frequency (γ being the usual relativistic factor), combined with the $1/R$ dependence of the primary vacuum toroidal field on the major radius, results in an approximate dependence $\gamma \propto 1/R$ of the resonant electron energy for vertical launching at a given frequency. In other words, resonant electrons are to be found at higher and higher energy as the beam moves towards the high field side of the tokamak.

The absorption of X3 waves in this configuration has been measured and found to be larger than that predicted by linear ray tracing calculations based on a Maxwellian distribution function [42]. The difference has been attributed to the generation of a suprathermal population by the X3 wave itself, which in turn gives rise to enhanced absorption of the wave. This suprathermal population is clearly detected by a high field side (HFS) second harmonic X-mode ECE radiometer, operating in the 78–114 GHz range with 24 channels of 0.75 GHz bandwidth. The ECE radiative temperature is in excess of that measured by a Thomson scattering diagnostic for the plasma bulk. In particular, by sweeping the beam from larger to smaller major radii, it is observed that the soft x-ray emission signal, which in all conditions observed in EC-heated plasmas in TCV is dominated by bremsstrahlung from thermal electrons and is thus related to the thermal energy, peaks at an earlier time than the characteristic ECE suprathermal signal [43]. At the time the latter reaches its maximum, most of the beam propagation occurs well away from the nominal (cold) X3 resonance region, indicating that absorption must occur on a high energy electron tail. The energy selectivity implied by the nearly one-to-one correspondence of major radius and energy opens the possibility of a particularly surgical form of distribution function engineering in velocity space, although the spatial localization of the absorption is poor in this case.

Earlier experiments were performed on TCV with one X3 beam injected through one of the lateral launchers intended for X2. These experiments were carried out in conjunction with X2 heating, which resulted again in a dramatic enhancement of the X3 first pass absorption efficiency with respect to linear modelling predictions. The absorption efficiency varied as a function of both the power and parallel wave number of the X2 waves, with up to 100% absorption measured in some cases [44]. The acceleration and sustainment of suprathermal electrons by X2 waves in an ECCD configuration, i.e. with a finite parallel wave vector, is well documented [45, 24] on TCV. In these experiments it was found that the variation of the X3 absorption efficiency mirrored that of the estimated total energy stored in the suprathermal population [46], strongly suggesting that the latter was responsible for the enhanced absorption. In both the lateral-launch and top-launch experiments, second-pass absorption due to wall reflection was estimated by steering the launching mirror away from the optimum angle and was found to be negligible [42, 44].

To quantify the deformation of the e.d.f. from a Maxwellian, a bi-Maxwellian model has been used for computational convenience; the e.d.f. in this model is the sum of a thermal and a suprathermal Maxwellian distribution. By constraining the spatial dependence of the density and temperature of the suprathermal component in accordance with hard x-ray measurements, the absolute values of both can be derived by a fit to the HFS ECE measurements [26]. For the X2/X3 experiments described above, this technique yielded suprathermal temperatures of the order of 12 keV (to be compared with 3 keV for the bulk) and suprathermal densities up to 24% of the bulk in the highest power case (1.5 MW X2 power). The calculated X3 absorption efficiency however still fell well short of the experimental value [26] (in a case with 100% measured absorption, the computed value was only 60%).

A better match to the available experimental observations is obtained by employing a slightly different *ad hoc* e.d.f. model, still convenient from a computational standpoint. This e.d.f. is built by adding two truncated Maxwellian functions: a bulk Maxwellian defined from 0 to a cutoff energy E_{cut} and a suprathermal Maxwellian defined from E_{cut} to infinity [47]. The difference between the two models is illustrated in figure 1. In this approach, the temperatures of the two components are both fixed, as functions of the radial coordinate, to the value given by Thomson scattering measurements for the bulk temperature and to the hard x-ray photon temperature for the suprathermal component, respectively. The bulk density is also measured by Thomson scattering. The free parameters are then E_{cut}, which determines the total suprathermal density, and the shape of the suprathermal density's radial profile.

From an analytical e.d.f. such as the one just described, the radiative ECE temperature can be calculated by using known electron cyclotron emission and absorption formulae [48] and propagating the emission along rays calculated by a WKB ray tracing code [47]. By employing a simple iterative approach and varying the free parameters, a good match can be obtained between the suprathermal density profile and the hard x-ray emission profile, reconstructed by inverting a multichord measurement of line integrated emission in the 30–40 keV range (see figure 2(*a*)—the matching is justified by the plasma parameters varying negligibly within the width of these narrow profiles), and between the measured and calculated radiative temperatures (see figure 2(*b*)), while also obtaining a significant absorption enhancement (above 80% in the case shown here, in which the measured value was 100%) [47]. The model has also the advantage of automatically guaranteeing consistency with the Thomson scattering measurements, as the energy dependence of the e.d.f. at low energy is completely independent of the assumed suprathermal temperature. While the sharp separation of the two populations is somewhat artificial, this simple model clearly demonstrates the compatibility of all experimental measurements with the attribution of the cause of the observed X2–X3 synergy to the suprathermal population.

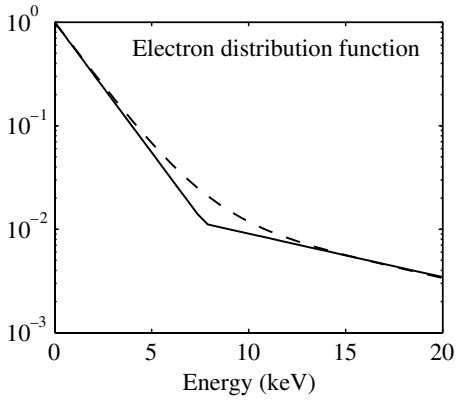

Figure 1. Model electron distribution functions: sum of truncated Maxwellians (solid curve), bi-Maxwellian (dashed curve).

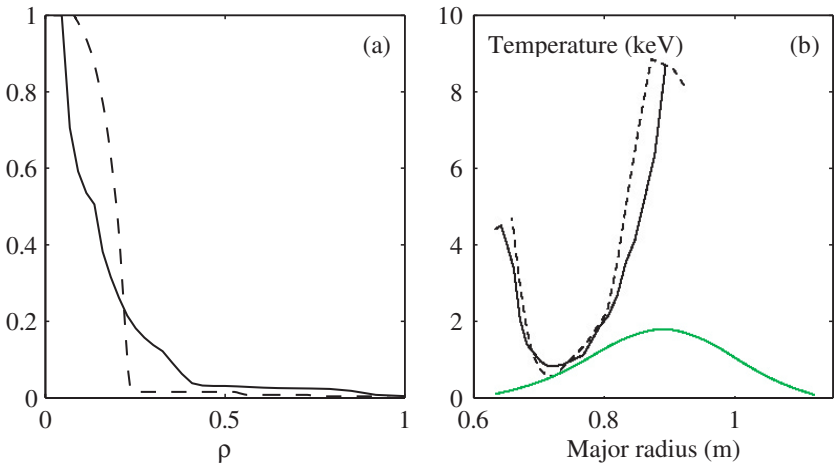

Figure 2. (*a*) Hard x-ray emissivity profile in the range 30–40 keV, derived with the Fisher regularization method [49] from the line integrated emission profile (solid curve), and modelled suprathermal density profile (dashed curve), in arbitrary units; (*b*) measured (solid curve) and modelled (dashed curve) radiative HFS ECE temperature, and bulk temperature (pale green curve) measured by Thomson scattering. Discharge with 1 MW lateral X3 heating and 0.3 MW X2 ECCD, injected with a toroidal angle of 14°; plasma current 200 kA, line-averaged density 1.8×10^{19} m^{-3}.

3. Transport of suprathermal electrons

The application of ECRH, and particularly ECCD, at extremely high power densities in TCV has led to the discovery of an important and hitherto largely ignored element in the dynamics of the e.d.f.: the cross-field transport of the current carrying suprathermal electrons [24]. Experimental estimates of the suprathermal transport level, generally expressed as a characteristic diffusivity, had been previously obtained primarily in lower hybrid heating experiments [50–52], although some cases with ECRH were also reported in the literature [29]. While the reported diffusivity values varied somewhat, they were generally smaller than or comparable to the bulk energy diffusivity. The resulting characteristic diffusion time scales, especially in large devices, were much longer than the slowing-down and pitch-angle scattering

time scales, allowing diffusion to be ignored. This also resulted in driven current profiles that closely followed the power deposition profile, with good general agreement between experiment and theory [4, 53].

This assumption clearly breaks down in TCV, where hard x-ray emission profiles are much broader than the ECRH power deposition [24]. Additionally, the total driven current is generally smaller than that calculated by Fokker–Planck modelling [54–56], which at these power levels exhibits a significant enhancement over the current computed by a linear Maxwellian model [57]. The discrepancy is however resolved when a radial diffusivity, typically of the order of or less than the electron energy diffusivity, is included in the Fokker–Planck model [56]. The motion of the suprathermal electrons away from the interaction region is the factor that inhibits the accumulation of acceleration events that would lead to strong nonlinear enhancement of the driven current. The result is a value of the current that is intermediate between linear and nonlinear predictions. In conditions under which no quasilinear enhancement would be expected even in the absence of transport (sufficiently low power density or sufficiently high plasma density), no significant difference in the total driven current is found when transport is included [55] (provided the broadening it causes does not become comparable to the device size). In a large fusion reactor such as ITER, transport effects can therefore be expected to be wholly negligible.

The limitation of quasilinear effects by transport represents a form of plasma self-regulation, since the quasilinear deformation of the e.d.f. and the effect of transport are *both* magnified as the power density increases, even if the transport itself remains constant. As electrons are driven to higher energies, their lifetime, i.e. the characteristic momentum destruction time, increases according to the classical collisional dependence $\tau \propto E^{3/2}$; the radial broadening caused by a diffusivity D is then $\sim (D\tau)^{1/2} \propto E^{3/4}$ [24]. An additional element of self-regulation could be introduced by a power degradation mechanism, i.e. an increase in the intrinsic transport with power owing to a rise in turbulence.

The occurrence of radial transport has been observed directly in TCV by employing a perturbative method based on the response of the HFS ECE to short, low duty cycle, periodic, localized X2 ECCD pulses [27]. The responsivity of ECE is enhanced by coherent averaging over up to 200 pulses within a single plasma discharge, in steady-state conditions. The ECCD pulses are applied with one or two 0.45 MW sources (with identical aiming) and are defined by a 0.2 ms ramp-up, a 0.25 ms flat top and a 0.1 ms ramp-down, with a periodicity of 8–10 ms. The pulse length has been empirically adjusted to be well below the time for quasilinear saturation, so that steady state is not reached, and to permit observation of the spatial propagation of the pulse after turn-off. The average power (<40 kW) is negligible compared with the cw input power even in Ohmic discharges, and the plasma can therefore be assumed not to be significantly affected by the power stimuli.

Resolving both the energy and the emission location in HFS ECE measurements is impossible in general. However, we can again adopt a simple bi-Maxwellian approximation in order to gain quantitative insight into the system dynamics. On the basis of the spatial dependence of the hard x-ray photon temperature, which is nearly invariably uniform, we may further assume that the suprathermal temperature T_s is independent of position. The variation of the radiative temperature with respect to its baseline value before the pulse can be expressed as [26]

$$T_r' = T_b' \exp(-\tau_s) + T_s[1 - \exp(-\tau_s)], \tag{1}$$

where T_b' is the variation in the temperature of the bulk, which is assumed to be optically thick, and τ_s is the optical thickness of the suprathermal component. The low average applied power allows us to make the assumption, verifiable *a posteriori*, that the suprathermal population is

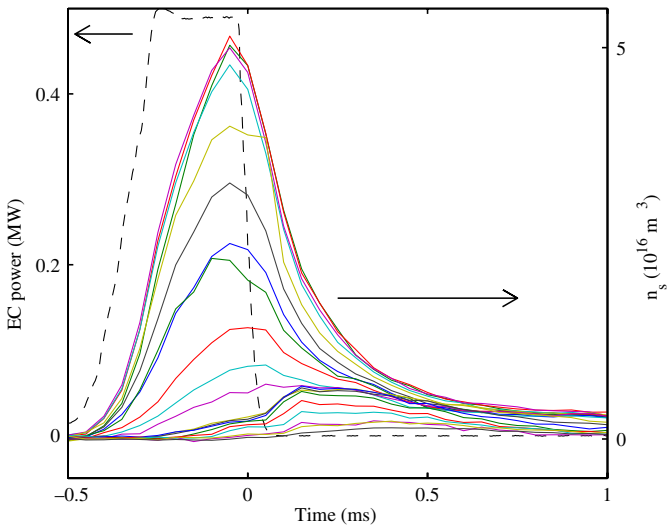

Figure 3. Time histories of suprathermal densities at different locations (spanning the range $\rho =$ 0–0.6, where ρ is a normalized radial coordinate proportional to the square root of the plasma volume), reconstructed from the HFS ECE signals and coherently averaged over multiple pulses (solid curves) and ECCD power (dashed curve). The power is applied near the magnetic axis, with a toroidal injection angle of 25°. Plasma current 230 kA, line-averaged density 1.5×10^{19} m^{-3}, no additional heating besides the ECCD pulses.

tenuous and optically thin, i.e. $\tau_s \ll 1$; in addition, by comparison with measurements of T_b by low field ECE, we find that $T_b' \ll T_r'$ [27], so that

$$T_r' \simeq T_s[1 - \exp(-\tau_s)]. \tag{2}$$

Finally, for a sufficiently narrow emissivity shape function, the suprathermal density n_s can be extracted through the formula [48] $\tau_s = 3.71\, n_s\, T_s\, R/B$ [10^{19} m^{-3}, keV, m, T], where R and B are the major radius and magnetic field, respectively, at the emissivity peak location. To first approximation, T_s can be inferred from the relativistic downshift of the symmetry point in the signal distribution, which is identified with the point of smallest minor radius along the ECE viewing chord. This then allows us to derive n_s from T_r'.

The time history for a case with central ECCD deposition is shown in figure 3. The outward propagation of the pulse is readily visible. A temperature $T_s \sim 11.5$ keV is inferred from the signal distribution. A simple measure of the radial propagation of the pulse is the time-to-peak (calculated from the power turn-off time), which is plotted in figure 4; to increase the radial range, data are gathered from four identical discharges with increasing vertical distance between the magnetic axis and the ECE chord. The abscissa for each shot is the emission location of downshifted radiation at $T_s = 11.5$ keV. The overlapping data are in satisfactory agreement, with most of the scatter attributed to density variations. The ray tracing code TORAY-GA [58] places the EC deposition in the region $\rho =$ 0–0.2, which is confirmed by the measurements to be a region of zero delay, within the ECE time resolution of 0.05 ms.

If the entire range of frequencies accessed by the radiometer is used, the time-to-peak as a function of frequency takes the form shown in figure 5 for four different values of the plasma density. The turnover and subsequent decrease in the time-to-peak with frequency in the high frequency range is attributed to third harmonic emission. Indeed, at those frequencies the cold plasma second harmonic emission layer moves to and beyond the edge of the plasma on the HFS, so that it becomes optically thin, allowing third harmonic radiation from the low field

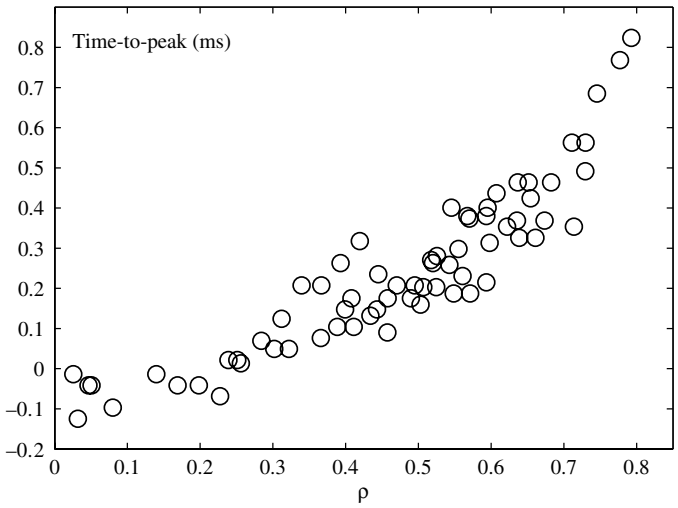

Figure 4. Time lag from the end of a central ECCD pulse to the ECE peak, as a function of ρ, calculated by taking into account the estimated relativistic downshift for a tail temperature of 11.5 keV. The discharge conditions are as in figure 3.

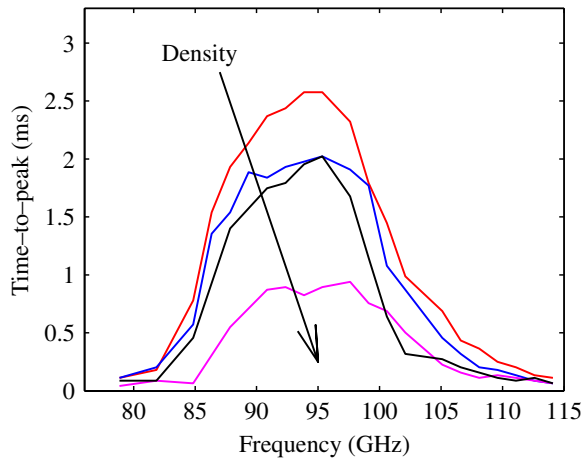

Figure 5. Time-to-peak as a function of HFS ECE frequency, for four discharges with line-averaged density equal to 0.4×10^{19} m^{-3}, 0.8×10^{19} m^{-3}, 1.05×10^{19} m^{-3} and 1.45×10^{19} m^{-3}, respectively, in the order indicated by the arrow. Plasma current 110 kA; 0.5 MW power is applied near the magnetic axis, with a toroidal injection angle of 25°.

side to shine through. As the frequency rises, this emission comes from regions increasingly closer to the centre, explaining the decrease in the time-to-peak towards zero.

The effect of radial transport on the shape of the suprathermal profile is rendered readily apparent by plotting successive snapshots of the normalized n_s profile after $t = 0$ (the power shut-off time), as shown in figure 6. A substantial broadening of the profile is clearly observed, occurring on a fast time scale of a few hundred microseconds. On the other hand, the decay of the absolute n_s profile at times well after the peak is quite slow, over 1 ms. By adopting a simple cylindrical model involving a spatial diffusivity D and a momentum destruction time τ, a fit to the data yields values of D in excess of 10 m^{2}s^{-1} and $\tau \sim$1.5 ms. This diffusivity

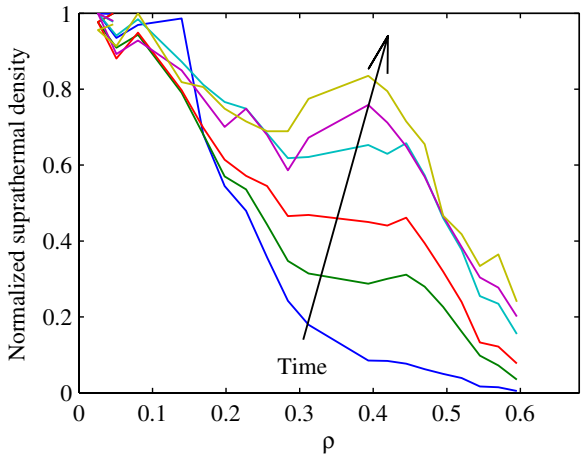

Figure 6. Normalized profiles of reconstructed suprathermal density at times 0, 0.1, 0.2, 0.3, 0.4 and 0.5 ms after the ECCD turn-off; the time order is as indicated by the arrow. The discharge is the same as in figure 3.

value lies above most previously reported measurements [50], as well as above the minimum values (0.3–5 m^2s^{-1}) required to explain the reduction of quasilinear effects in the driven current [56]. However, we note in passing that in a TCV study of suprathermal electrons (of 10–15 keV energy) accelerated by the electric fields generated by sawtooth crashes, their radial diffusivity has been estimated to be of the order of 25 m^2s^{-1} [47].

The fitted value of τ, when equated to a classical collisional momentum destruction time, is consistent with electrons of energy greater than 50 keV. This is in disagreement with the initial assumption of a suprathermal temperature of 11.5 keV, which can only be a reflection of the simplicity of the model. Indeed, on a fast time scale the assumption of a uniform suprathermal temperature is doubtful, as electrons of different energy will travel different distances and may also diffuse at different underlying rates. However, the long decay time and the rapid broadening of the suprathermal profile cannot be explained other than by rapid transport of high energy electrons. The strong decrease in the time-to-peak with density (figure 5) is also a reflection of the role of the momentum destruction time in the system dynamics. Simulations of this experiment with a full Fokker–Planck model will be required to reconstruct the e.d.f. dynamics in more quantitative detail.

4. Conclusions

The physics of wave–plasma interaction in the electron cyclotron range of frequencies permits targeting of specific regions of phase space by ECRH. As a consequence of this property, and owing to the significant associated technological development, ECRH has progressively evolved from a straightforward bulk heating tool to a precision electron distribution function manipulation tool. Numerous achievements have been documented in recent years in the realms of stability control, confinement enhancement and current profile tailoring and sustainment.

The modification of the e.d.f. induced by ECRH has also been employed to further affect the wave–plasma interaction and enhance the wave damping. Experiments on TCV have shown that a significant enhancement of first-pass absorption of third harmonic ECRH is obtained in the presence of a suprathermal electron population, excited by either the third

harmonic wave itself or by second harmonic ECCD. A simple two-population model for the e.d.f. succeeds in reproducing the enhanced absorption as well as all available experimental measurements.

These efforts have progressed in parallel with an increased understanding of the underlying physics, particularly in relation with the relaxation dynamics of the e.d.f.. The increase in electron energy that accompanies an increase in ECCD power also extends the lifetime of the energetic electrons and allows them to escape the wave interaction region through cross-field transport, preventing further acceleration. This self-regulation effect sets an upper asymptotic limit to ECCD efficiency and completes a theoretical picture that is already well understood in the low power density regime relevant to a fusion reactor. A concrete visualization of the dynamical response of the e.d.f. to ECRH is obtained by perturbative studies using ECE, confirming the fundamental role of spatial transport at high power and further suggesting an increase in the level of transport with power itself. By progressively constraining the interpretation, this concerted body of work holds out the promise of an increasingly quantitative characterization of the e.d.f. evolution in strongly driven and turbulent plasma systems.

Acknowledgment

This work was supported in part by the Swiss National Science Foundation.

References

[1] Bernabei S *et al* 1982 *Phys. Rev. Lett.* **49** 1255
[2] Alberti A *et al* 2001 *Fusion Eng. Des.* **53** 387
[3] Dammertz G *et al* 2006 *IEEE Trans. Plasma Sci.* **34** 173
[4] Prater R 2004 *Phys. Plasmas* **11** 2349
[5] Luce T C *IEEE Trans. Plasma Sci.* **30** 734
[6] Erckmann V and Gasparino U 1994 *Plasma Phys. Control. Fusion* **36** 1869
[7] Pietrzyk Z A *et al* 2000 *Phys. Plasmas* **7** 2909
[8] Henderson M A *et al* 2003 *Phys. Plasmas* **10** 1796
[9] Angioni C, Goodman T P, Henderson M A and Sauter O 2003 *Nucl. Fusion* **43** 455
[10] Gantenbein G, Zohm H, Giruzzi G, Günter S, Leuterer F, Maraschek M, Meskat J, Yu Q, ASDEX Upgrade Team and ECRH-Group (AUG) 2000 *Phys. Rev. Lett.* **85** 1242
[11] Prater R, LaHaye R J, Lohr J, Luce T C, Petty C C, Ferron J R, Humphreys D A, Strait E J, Perkins F W and Harvey R W 2003 *Nucl. Fusion* **43** 1128
[12] Sauter O *et al* 2000 *Phys. Rev. Lett.* **84** 3322
[13] Henderson M A, Camenen Y, Coda S, Goodman T P, Nikkola P, Pochelon A, Sauter O and TCV Team 2004 *Phys. Rev. Lett.* **93** 215001
[14] Coda S *et al* 2005 *Phys. Plasmas* **12** 056124
[15] Fisch N J and Boozer A H 1980 *Phys. Rev. Lett.* **45** 720
[16] Giruzzi G *et al* 2004 *Proc. 20th Conf. on Fusion Energy (Vilamoura, Portugal, 2004)* (Vienna: IAEA) CD-ROM file EX/P4-22 and http://www-pub.iaea.org/MTCD/Meetings/PDFplus/fusion-20-preprints/index.htm
[17] Ohkawa T 1976 *General Atomics Report* GA-A13847
[18] Decker J 2003 *Proc. 15th Topical Conf. on Radio Frequency Power in Plasmas (Moran) AIP Conf. Proc.* **694** 447
[19] Von Goeler S *et al* 1985 *Nucl. Fusion* **25** 1515
[20] Texter S, Knowlton S, Porkolab M and Takase Y 1986 *Nucl. Fusion* **26** 1279
[21] Peysson Y and Imbeaux F 1999 *Rev. Sci. Instrum* **70** 3987
[22] Da Cruz DF, Jr, Meijer J H and Donné A J H 1992 *Rev. Sci. Instrum.* **63** 5026
[23] Kawashima H, Hasegawa M, Fuchs G, Matoba T, Uesugi Y, Hoshino K, Kawakami T and Yamamoto T 1994 *Japan. J. Appl. Phys.* **33** 3590
[24] Coda S, Alberti S, Blanchard P, Goodman T P, Henderson M A, Nikkola P, Peysson Y and Sauter O 2003 *Nucl. Fusion* **43** 1361

[25] Coda S, Alberti S, Blanchard P, Goodman T P, Henderson M A, Nikkola P, Peysson Y and Sauter O 2002 *Proc. 29th EPS Conf. on Controlled Fusion and Plasma Physics (Montreux)* vol 26B (ECA) O-4.03 and http://epsppd. epfl.ch/Montreux/start.htm
[26] Blanchard P, Alberti S, Coda S, Weisen H, Nikkola P and Klimanov I 2002 *Plasma Phys. Control. Fusion* **44** 2231
[27] Coda S, Alberti S, Blanchard P, Klimanov I, Moret J-M and Weber P 2003 *Proc. 30th EPS Conf. on Controlled Fusion and Plasma Physics (St. Petersburg, Russia)* vol 27A (ECA) P-3.134 and http://epsppd.epfl.ch/StPetersburg/start.html
[28] Luce T C, Efthimion P C and Fisch N J 1988 *Rev. Sci. Instrum.* **59** 1593
[29] Giruzzi G, Steimle R F, Roberts D R, Sing D and Wootton A J 1996 *Plasma Phys. Control. Fusion* **38** 1593
[30] Preische S, Efthimion P C and Kaye S M 1996 *Phys. Plasmas* **3** 4065
[31] Zhuang G, Behn R, Klimanov I, Nikkola P and Sauter O 2005 *Plasma Phys. Control. Fusion* **47** 1539
[32] Krivenski V 2001 *Fusion Eng. Des.* **53** 23
[33] Uehara K, Tsushima A, Amemiya H, Kawasima H and Hoshino K 2003 *Japan. J. Appl. Phys.* **42** 657
[34] Iwamae A, Sato T, Horimoto Y, Inoue K, Fujimoto T, Uchida M and Maekawa T 2005 *Plasma Phys. Control. Fusion* **47** L41
[35] Giruzzi G 1988 *Phys. Fluids* **31** 3305
[36] Harvey R W and McCoy M G 1992 *Proc. IAEA Technical Committee Meeting on Advances in Simulation and Modeling in Thermonuclear Plasmas (Montreal)* (Vienna: IAEA) p 498
[37] O'Brien M R, Cox M, Warrick C D and Zaitsev F S 1992 *Proc. IAEA Technical Committee Meeting on Advances in Simulation and Modeling in Thermonuclear Plasmas (Montreal)* (Vienna: IAEA) p 527
[38] Kamendje R, Kasilov S V, Kernbichler W and Heyn M F 2003 *Phys. Plasma* **10** 75
[39] Hofmann F *et al* 1994 *Plasma Phys. Control. Fusion* **36** B277
[40] Goodman T P *et al* 2003 *Nucl. Fusion* **43** 1619
[41] Hogge J-P, Alberti S, Porte L and Arnoux G 2003 *Nucl. Fusion* **43** 1353
[42] Alberti S, Arnoux G, Porte L, Hogge J-P, Marletaz B, Marmillod P, Martin Y, Nowak S and TCV Team 2005 *Nucl. Fusion* **45** 1224
[43] Arnoux G, Alberti S, Porte L, Nelson-Melby E, Hogge J-P and TCV Team 2005 *Plasma Phys. Control. Fusion* **47** 295
[44] Alberti S *et al* 2002 *Nucl. Fusion* **42** 42
[45] Coda S *et al* 1999 *Proc. 26th EPS Conf. on Controlled Fusion and Plasma Physics (Maastricht, The Netherlands)* vol 23J (ECA) p 1097 and http://epsppd.epfl.ch/Maas/web/index.htm
[46] Coda S, Peysson Y, Alberti S, Goodman T P, Henderson M A, Nikkola P and Sauter O 2001 *Proc. 28th EPS Conf. on Controlled Fusion and Plasma Physics (Funchal)* vol 25A (ECA) p 301 and http://epsppd.epfl.ch/Maas/web/index.htm
[47] Klimanov I 2006 *PhD Thesis* Ecole Polytechnique Fédérale de Lausanne, No. 3432, Lausanne, Switzerland
[48] Bornatici M, Cano R, De Barbiere O and Engelmann F 1983 *Nucl. Fusion* **23** 1153
[49] Frieden B R 1988 *J. Mod. Opt.* **35** 1297
[50] Peysson Y 1993 *Plasma Phys. Control. Fusion* **35** B 253
[51] Texter S, Porkolab M, Bonoli P T, Knowlton S and Takase Y 1993 *Phys. Lett.* A **175** 428
[52] Giruzzi G, Ségui J L, Dudok de Wit T, Michelot Y, Peysson Y, Moreau D and Talvard M 1995 *Phys. Rev. Lett.* **74** 550
[53] Petty C C, Lin-Liu Y R, Luce T C, Makowski M A, Prater R, Schuster D I, St. John H E and Wong K L 2001 *Nucl. Fusion* **41** 551
[54] Coda S *et al* 2000 *Plasma Phys. Control. Fusion* **42** B311
[55] Harvey R W, Sauter O, Prater R and Nikkola P 2002 *Phys. Rev. Lett.* **88** 205001
[56] Nikkola P, Sauter O, Behn R, Coda S, Condrea I, Goodman T P, Henderson M A, Harvey R W and the TCV Team 2003 *Nucl. Fusion* **43** 1343
[57] Harvey R W, McCoy M G and Kerbel G D 1989 *Phys. Rev. Lett.* **62** 426
[58] Matsuda K 1989 *IEEE Trans. Plasma Sci.* **17** 6